Letter

Dominant role of charge ordering on high harmonic generation in $Pr_{0.6}Ca_{0.4}MnO_3$

A. Nakano [1,*] K. Uchida [1] Y. Tomioka,[2] M. Takaya [3] Y. Okimoto [4] and K. Tanaka [1,5,†]

[1]*Department of Physics, Graduate School of Science, Kyoto University, Kyoto 606-8502, Japan*

[2]*National Institute of Advanced Industrial Science and Technology (AIST), Tsukuba 305-8565, Japan*

[3]*Department of Geology and Mineralogy, Graduate School of Science, Kyoto University, Kyoto 606-8502, Japan*

[4]*Department of Chemistry, Tokyo Institute of Technology, Meguro, Tokyo 152-8551, Japan*

[5]*Institute for Integrated Cell-Material Sciences, Kyoto University, Sakyo-ku, Kyoto 606-8501, Japan*

(Received 14 September 2023; revised 25 May 2024; accepted 31 July 2024; published 31 October 2024)

High harmonic generation (HHG) is a typical high-order nonlinear optical phenomenon and can be used to probe electronic structures of solids. Here, we investigate the temperature dependence of HHG from $Pr_{0.6}Ca_{0.4}MnO_3$ in the range of 7–294 K, including the charge ordering (CO) transition and magnetic transition temperatures. The high harmonic (HH) intensity remains almost constant in the high-temperature charge-disordered phase. However, as the temperature is lowered, it starts to increase near the CO transition temperature where an optical gap related to the CO appears. The anomalous gap energy dependence resembles the one recently reported in a Mott insulator. We attribute the suppression of the HH intensity at high temperatures to the destructive interference among HH emissions from thermally activated multiple charge configurations. Our results suggest that HHG is a promising tool for probing the fluctuation of local order in strongly correlated systems.

DOI: 10.1103/PhysRevResearch.6.L042032

High-order harmonic generation (HHG) is typical of nonperturbative nonlinear optical phenomena where the energy scale of the light-matter interaction reaches the typical energy scale of the material. An early report of HHG in a nonperturbative regime was in a gas material [1]. After the nonperturbative HHG in a bulk solid was reported by Ghimire *et al.* [2], this extreme nonlinear phenomenon has attracted attention from not only researchers in atomic and molecular physics but also those in condensed matter physics.

The origin of HHG is attributed to sublaser-cycle carrier dynamics driven by the electric field of the laser. In crystalline solids, the high harmonics (HHs) originate from the motion of Bloch electrons in a periodic potential, meaning that HHG measurements allow us to probe the properties of the material [2–9]. For example, the momentum-dependent band gap of ZnO along the Γ-*M* direction was reconstructed by using HHs from a two-color laser pulse [5].

The HHG process in typical semiconductors can be intuitively understood by a semiclassical three-step model like that in atomic gasses [10], consisting of Zener tunneling, acceleration, and recombination of Bloch electrons [11–13]. However, this simple picture does not necessarily hold in strongly correlated systems (SCSs) because the strong coupling of charge with multiple degrees of freedom modifies the charge dynamics driven by the laser field, which emits HHs. Although authors of many theoretical studies have predicted unique aspects of HHG in SCSs [14–21], only a few experiments have been performed [22–24].

A recent HHG measurement of a Mott insulator Ca_2RuO_4 has demonstrated that HHG in SCSs offers unique nonlinear optical phenomena peculiar to SCSs and has the potential to probe many-body states in SCSs [24]. In the measurement, the intensity of the harmonics increased as the gap energy increased with decreasing temperature. This is contrary to what one would intuitively expect from the three-step model, where the tunneling probability should be smaller as the gap energy increases. This unusual gap energy dependence was qualitatively reproduced in the simulation of a single-band Hubbard model at finite temperatures [21]. The authors of Ref. [21] proposed a scenario that the temperature-dependent spin background affects the charge dynamics through spin-charge coupling as follows: In the ground state, the spins are arranged antiferromagnetically (AFM). That is, if one site has an electron with spin up, the next neighboring site should have an electron with spin down at the ground state. As the temperature of the system gets higher, more spin configurations different from the AFM ordered ground state are thermally activated. Considering that there is spin-charge coupling, the emitted light resulting from the charge motion would have different phases for different spin configurations. Therefore, the destructive interference of HH emissions from thermally disturbed multiple spin configurations may suppress the HH intensity at finite temperatures.

The above scenario is not restricted to the materials with spin-charge coupling but could apply more generally to

*Contact author: nakano.aiko.75n@st.kyoto-u.ac.jp

†Contact author: kochan@scphys.kyoto-u.ac.jp

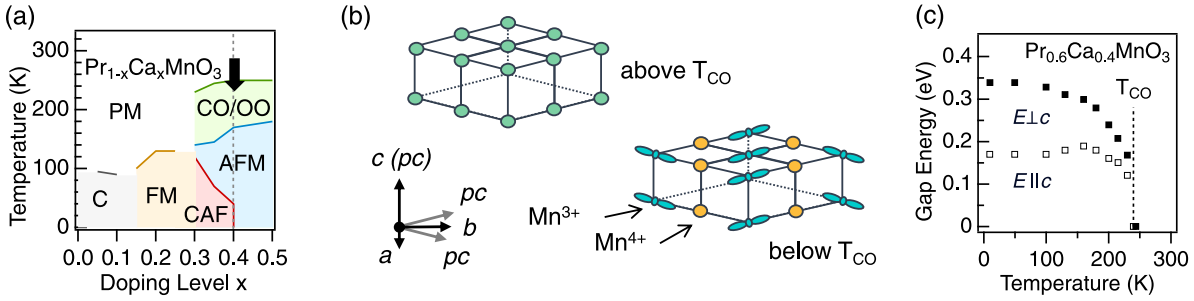

FIG. 1. Several ordered phases in $Pr_{1-x}Ca_xMnO_3$. (a) Magnetic and electronic phase diagram as a function of doping level x. PM, C, and FM denote the paramagnetic, spin-canted, and ferromagnetic phases, respectively. For $0.3 \leqslant x \leqslant 0.5$, the antiferromagnetic (AFM) insulating phase exists in the charge-orbital ordered (CO/OO) phase. The canted-AFM (CAF) phase also appears for $0.3 \leqslant x \leqslant 0.4$ (from Ref. [30]). (b) Schematic pictures of charge and orbital arrangements in the charge disordered (above T_{CO}) and charge ordered (below T_{CO}) states in $Pr_{0.6}Ca_{0.4}MnO_3$. Below T_{CO}, checkerboard charge ordering appears accompanied by the e_g-orbital ordering within the orthorhombic ab plane, as shown in fig. 3 in Ref. [25] (arrangements of spins are omitted). (c) Temperature dependence of the gap energy previously reported (reprinted with permission from Ref. [33]).

materials where other degrees of freedom are coupled to charge dynamics. A material with a charge-ordered phase is an attractive candidate to verify the universality of the scenario. In its charge-ordered ground state, charges are periodically localized in space. As in the case of the AFM phase, the charge configuration is thermally disturbed and deviates from the ground state at finite temperatures. If the charge ordering (CO) is strongly coupled with the charge dynamics, this system may exhibit HHG properties like those reported for the Mott insulator [21].

In this letter, we report on the temperature-dependent properties of HHG in manganese oxide with several electronic phases including the charge-ordered phase. Our purpose is to clarify the effect of the couplings of the charge dynamics with the multiple degrees of freedom on HHG.

$Pr_{1-x}Ca_xMnO_3$ is a prototypical system that exhibits CO. It has an orthorhombically distorted perovskite structure composed of transition metal ions surrounded by oxygen octahedra around Mn ions. At room temperature, the crystal structure is slightly distorted and is almost like a cubic ($a \approx b \approx c/\sqrt{2}$), so it is also called pseudocubic. It exhibits various magnetic and electronic phases depending on the valance of the transition metal ions, temperature, and the presence of external magnetic or electric fields [25–29]. Figure 1(a) shows the magnetic and electronic phase diagram of $Pr_{1-x}Ca_xMnO_3$ ($x = 0$-0.5) as a function of x [30]. These phases result from the couplings between spin, orbital, and charge degrees of freedom [31,32].

We chose the hole-doping level of $x = 0.4$ to investigate the effect of the electronic phase on the properties of HHG. As indicated by the black arrow in the phase diagram [Fig. 1(a)], $Pr_{0.6}Ca_{0.4}MnO_3$ is a charge-disordered paramagnetic insulator (PI) at room temperature and undergoes three successive phase transitions at T_{CO}, T_N, and T_C to phases that are called CO, AFM, and canted-AFM (CAF), respectively [30]. The checkerboard CO pattern in the ab plane (in the orthorhombic $Pbnm$ setting) below the CO transition temperature $T_{CO} \approx 240$ K is illustrated schematically in Fig. 1(b). The transition metal cations with different valency Mn^{3+} and Mn^{4+} are placed alternately in the orthorhombic ab plane. The CO accompanies orbital ordering (OO) where Mn e_g orbitals align within the orthorhombic ab plane, as shown in the right side of Fig. 1(b). Thus, this phase is denoted as the CO/OO (charge-orbital ordered) phase in Fig. 1(a). In the following, we call this phase the CO phase. $Pr_{0.6}Ca_{0.4}MnO_3$ exhibits an optical gap $2\Delta(T)$ below T_{CO}, and it increases with lowering temperature, as shown in Fig. 1(c) [33]. The origin of the gap opening is the intersite Coulomb repulsion between neighboring Mn ion sites, leading to CO formation [34].

The HHG measurements were performed with midinfrared (MIR) pulses with a photon energy $\hbar\omega_0$ of 0.26 eV, repetition rate of 1 kHz, pulse duration of 100 fs, and intensity of $0.3\,\mathrm{TW/cm^2}$ at the sample surface. Figure 2(a) shows the schematic configuration of the experimental setup in reflection geometry (details are shown in Fig. S1 in the Supplemental Material [35]). The power of the MIR light was controlled by a pair of wire-grid (WG) polarizers. The polarization direction of the MIR light was controlled by a combination of a liquid crystal retarder (LCR) as a quarter-wave plate and a WG polarizer. The MIR light was focused on the sample using a reflective objective lens with the 20° angle of incidence. Indium tin oxide (ITO)-coated glass was placed as a mirror that reflects the MIR light and transmits visible light.

The $Pr_{0.6}Ca_{0.4}MnO_3$ bulk crystal was mounted in a cryostat, whose temperature was controlled from 7 to 294 K with an accuracy of ~1 K. This allowed us to compare the HHG properties in several electronic and magnetic phases which include PM, CO, AFM, and CAF. From the reflectance measurement of the MIR light, we confirmed that the temperature dependence of the Fresnel losses of the incident light is negligible (<20%) for our discussion on temperature-dependent HHG (for more information on the reflectance measurement, see Sec. S2 in the Supplemental Material [35], including Ref. [36]).

Figure 2(b) is an optical image of the sample surface. Two pseudocubic axes pc_1 and pc_2 corresponding to Mn-O bonds are in the surface plane. One of the pseudocubic axes pc_1 is parallel to the c axis, and the other one pc_2 is perpendicular to the c axis (see Sec. S3 in the Supplemental Material [35], including Ref. [36]). The crystal was grown using the floating zone (FZ) method. The surface roughness was reduced to < 1 μm by polishing and buffing.

Figure 2(c) shows the HH spectra measured at two temperatures, at 294 K above T_{CO} (black dashed line) and at

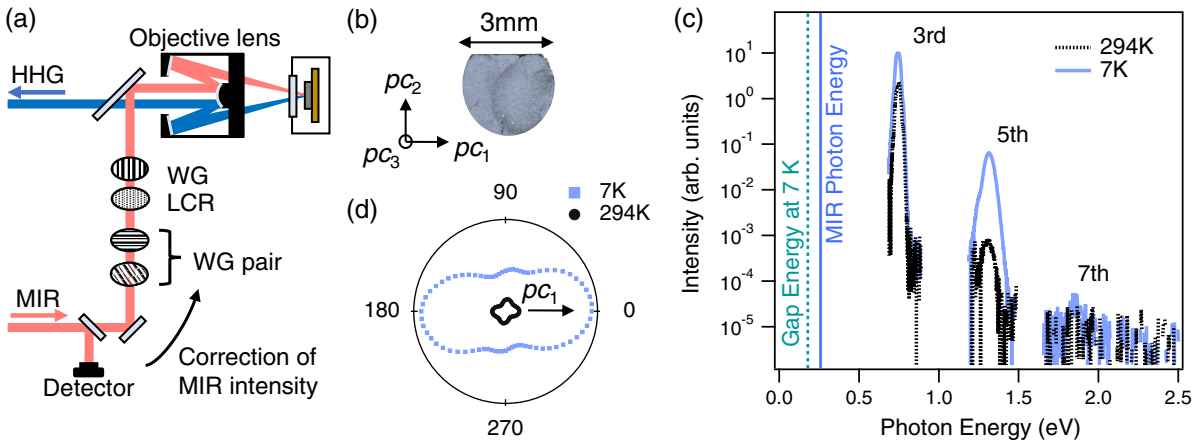

FIG. 2. High harmonic generation (HHG) in $Pr_{0.6}Ca_{0.4}MnO_3$. (a) Schematic configuration of the HHG measurement in reflection geometry. WG and LCR denote wire-grid polarizer and liquid crystal retarder, respectively. (b) Optical image of $Pr_{0.6}Ca_{0.4}MnO_3$ bulk sample. (c) High harmonic (HH) spectra were obtained at 7 K (blue solid line) and 294 K (black dashed line) with the midinfrared (MIR) light linearly polarized along the pc_1 axis. The MIR photon energy (0.26 eV) indicated by the blue solid line is a little higher than the gap energy at the ground state (0.18 eV) shown by the green dashed line. (d) Polar plots of the third harmonic intensity as a function of the polarization angle θ of the MIR excitation light. It takes local maximum values when the MIR polarization is in the direction of the Mn-O bonds ($\theta = 0°$, 90°, 180°, and 270°).

7 K below T_C (blue solid line), with the MIR intensity of 0.3 TW/cm^2 and polarization along the pc_1 axis. The emissions of the third and fifth harmonics were observed at 294 K and the seventh harmonics at 7 K. Even-order harmonics were not observed at all temperatures, although inversion symmetry is broken below T_{CO}. This missing may be due to the microtwin structure of the sample. As for symmetry analysis of HHG, see Sec. S4 in the Supplemental Material [35], including Refs. [37–39]. The HH intensity result indicates that phase transition causes a drastic change in the HHG properties.

Figure 2(d) shows polar plots of the third harmonic intensity as a function of the MIR polarization angle at 294 K above T_{CO} (the black plots in the center) and at 7 K below T_C (the blue plots). The polarization angle θ of the MIR light was rotated with respect to the pc_1 axis ($\theta = 0$ indicates linearly polarized MIR light along pc_1). At 294 K, the HH emission is larger along the two pseudocubic directions, exhibiting almost fourfold symmetry reflecting pseudocubic lattice structure. The monotonic increase of the HH emission with lowering temperature is the same along both axes, but the rate of change is different. At 7 K, the HH emission is much more enhanced along pc_1 than along pc_2, exhibiting twofold symmetry reflecting structural transition from pseudocubic to a lower symmetry (pseudo-orthorhombic) phase below T_{CO} (more information on the orientation dependence of the third harmonic intensity is in Sec. S5 in the Supplemental Material [35]). In the following, we will focus on the HHG results with linearly polarized MIR light excitation along the pc_1 axis ($\theta = 0°$). Along the pc_1 axis, the temperature-dependent gap energy is always relatively smaller than the MIR photon energy (0.26 eV) at any temperature [see Fig. 1(c)].

Figure 3 shows the MIR intensity dependence of the HHG yields. In all other experiments, we set the MIR intensity to 0.3 TW/cm^2, where the electric field strength is 10 MV/cm (in air). It is sufficiently strong to induce the large amplitude of charge motion and enable the HHG to enter the nonperturbative regime. The third and fifth harmonic intensities are approximately proportional to I_{MIR}^m with $m = 1.9$ (third) and $m = 2.7$ (fifth), respectively. These values are deviated from that in a perturbative regime ($m = n$ for nth harmonics), indicating the direct evidence for a nonperturbative regime (for more details, see Sec. S6 in the Supplemental Material [35], including Refs. [2,3,40,41]).

To further investigate the relationship between HH intensities and material phases, we measured detailed temperature dependences, as shown in Figs. 4(a) and 4(b). The HH

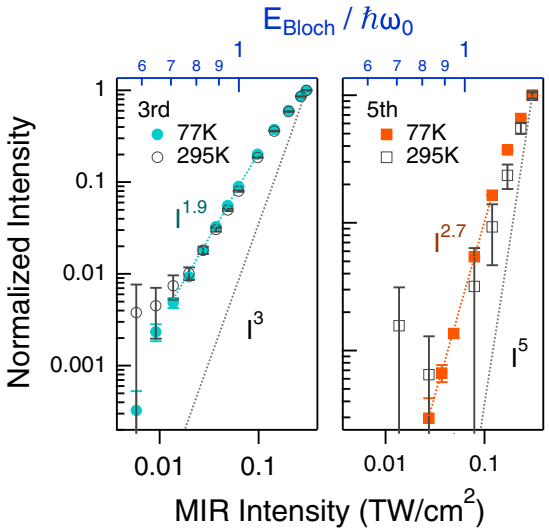

FIG. 3. Midinfrared (MIR) intensity dependence of the high harmonic (HH) intensity above and below T_{CO} (295 and 77 K). The third (left panel) and fifth (right panel) harmonic intensities are plotted as a function of MIR intensity. The harmonic intensities are normalized by the values at the highest MIR intensity. The open markers are measured at 295 K, and the solid markers are measured at 77 K. The top axes of each panel are the ratio of Bloch energy E_{Bloch} to the photon energy of the incident light $\hbar\omega_0$. See Sec. S6 in the Supplemental Material [35], including Refs. [2,3,40,41], for their definitions and further discussion.

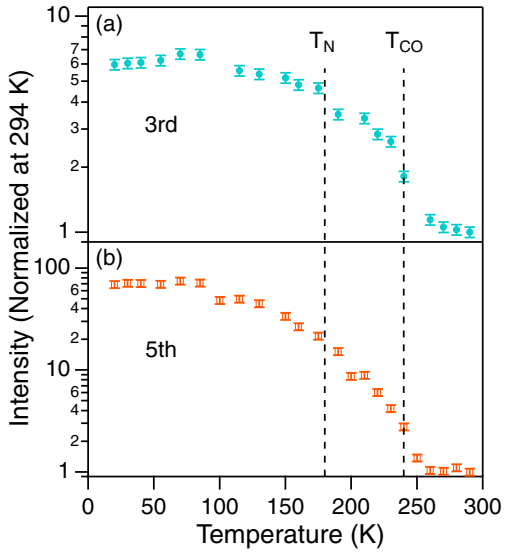

FIG. 4. Enhancement of high harmonic generation (HHG) below T_{CO} under midinfrared (MIR) with the polarization angle $\theta = 0°$. The temperature-dependent intensities of the (a) third and (b) fifth harmonics normalized at 294 K. The dashed lines at 240 and 180 K indicate the charge-orbital ordering transition temperature (T_{CO}) and Néel temperature (T_N), respectively. Error bars are estimated by considering the fluctuations of the power of the MIR excitation light during the measurement.

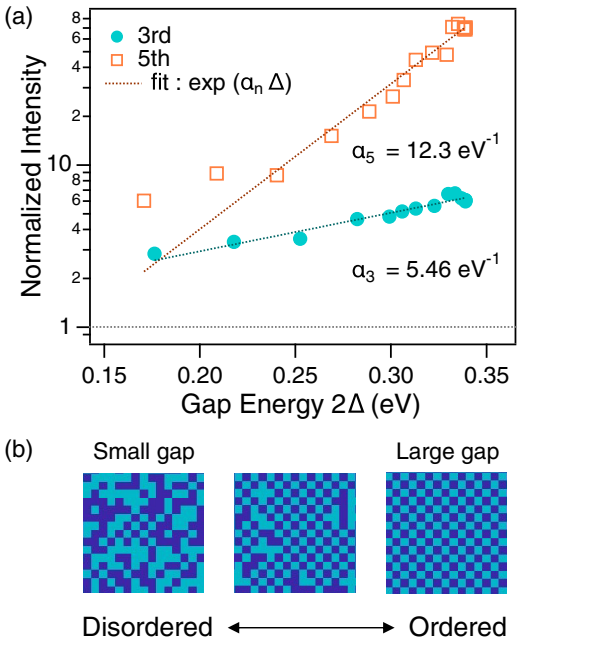

FIG. 5. (a) Gap energy dependence of the high harmonic (HH) intensity below T_{CO}. The intensities of the third (closed circle) and fifth (open square) harmonics are normalized at 294 K. Here, α_3 and α_5 are fitting parameters for each line. (b) Snapshots of charge configuration within the orthorhombic *ab* plane with small gap energy (left side) to large gap energy (right side).

intensity remains at almost the same value in the PI phase above T_{CO}. On the other hand, it starts to increase as the temperature is lowered below T_{CO}. No noticeable change takes place around the magnetic phase transition temperatures T_N or T_C. Therefore, we conclude that the CO, rather than the magnetic ordering, strongly influences HHG in $Pr_{0.6}Ca_{0.4}MnO_3$.

The gap energy 2Δ for $E \perp c$ ($\theta = 90°$) could be a good indicator of charge order. As plotted by filled squares in Fig. 1(c), it decreases monotonically with increasing temperature and is not affected by AFM spin ordering at T_N [33]. This temperature dependence of $2\Delta(T)$ reflects that thermal activation of charge configurations different from the ground state suppresses the CO with increasing temperature.

To reveal the relationship between the HH emission process and charge order, we plot the HH intensity (third harmonics: filled circles; fifth harmonics: open squares) as a function of the gap energy, as shown in Fig. 5(a) using temperature dependences of the HH intensity and the gap energy [33]. We found that the HH intensity increases almost exponentially as the gap energy increases. We performed the fitting of the nth-order harmonic intensity with $I_n(\Delta) = I_n(0)\exp(\alpha_n\Delta)$ using an exponent of α_n as the fitting parameter [dashed lines in Fig. 5(a)]. The larger value of $\alpha_5 = 12.3$ eV^{-1} than $\alpha_3 = 5.46$ eV^{-1} indicates the stronger correlation between higher nonlinear optical response and the CO. The relationship between HH intensity and the gap energy resembles those found in a previous experimental study on the Mott insulator Ca_2RuO_4 [24] and theoretical study in half-filled Mott-Hubbard model [21], in which the exponent is larger for higher harmonics.

The important difference between the previous theoretical study (Ref. [21]) and this letter is whether the mechanism of the gap opening depends on the spin ordering or not. In $Pr_{0.6}Ca_{0.4}MnO_3$, it is reasonable to suppose that thermally disturbed charge configurations [see Fig. 5(b)] play a role like thermally disturbed AFM spin configurations in a Mott insulator. Our results imply that the scenario proposed by Murakami *et al.* [21] applies not only to spin systems but also to systems with CO which is unrelated to spin ordering. That is, the temperature-dependent charge order and its fluctuation affects the charge dynamics as follows: As the temperature of the system becomes higher in the CO phase, more configurations different from the charge ordered state are thermally activated, where the CO region is shrunk, as shown in the left panel of Fig. 5(b). In this material, there exists a strong coupling between the local charge configuration and an itinerant electron. Consequently, each of the charge configurations can modulate the motion of the charge driven by an electric field, differently. Then the emitted light resulting from the charge motion would have different phases for different configurations. Thus, the destructive interference of HH emissions from thermally disturbed multiple charge configurations may suppress the HH intensity at finite temperatures. Finally, above T_{CO}, where CO disappears and any charge configurations are allowed, HH intensity becomes independent of temperature observed in our experiment.

Such a sensitivity of HHG to the fluctuation of local order in SCSs is no surprise. Authors of a recent study have succeeded in the reconstruction of the valence band and electron density with a spatial resolution of the order of several tens of picometers, using HHs [9]. Authors of another theoretical study showed that the disorder of the atomic arrangement suppresses the HH intensity in solids [42]. These studies indicate

that HHG is sensitive to the local structure with atomic-scale resolution. Our claim is consistent with these previous studies: HHG can be a probing tool for the fluctuation of local order in SCSs. Further comprehensive experimental and theoretical studies may lead to a deeper understanding of the physics behind the observed results, including the microscopic mechanism.

In summary, we performed HHG measurements in $Pr_{0.6}Ca_{0.4}MnO_3$ over a wide range of temperatures. We found that the charge disordering to CO transition drastically changes the properties of HHG. Below T_{CO}, we encountered an anomalous gap energy dependence of the HH intensity which resembles the one found in the Mott insulator Ca_2RuO_4 [24]. The resemblance between our experimental results and those reported for Ca_2RuO_4 suggests that a scenario like the one proposed by Murakami *et al.* [21] may occur in a variety of ordered phases in SCSs whether spin ordering is involved or not. We concluded that the main factor in the suppression of the HH intensity at high temperatures in our measurements is the strong coupling between the charge configuration and the charge dynamics. Our results provide additional evidence for the applicability of HHG as a probing tool for the fluctuation of local order in SCSs.

A.N. and K.U. are thankful to Yuta Murakami for fruitful discussions. This letter is supported by Grants-in-Aid for Scientific Research (S) (Grants No. JP21H05017 and No. JP17H06124) and Grants-in-Aid for Scientific Research (C) (Grant No. JP22K03484). A.N. is thankful for JST SPRING (Grant No. JPMJSP2110). K.U. is thankful for a Grant-in-Aid for Challenging Research (Pioneering) (Grant No. JP22K18322).

[1] M. Ferray, A. L'Huillier, X. F. Li, L. A. Lompre, G. Mainfray, and C. Manus, Multiple-harmonic conversion of 1064 nm radiation in rare gases, J. Phys. B **21**, L31 (1988).

[2] S. Ghimire, A. D. DiChiara, E. Sistrunk, P. Agostini, L. F. DiMauro, and D. A. Reis, Observation of high-order harmonic generation in a bulk crystal, Nat. Phys. **7**, 138 (2011).

[3] O. Schubert, M. Hohenleutner, F. Langer, B. Urbanek, C. Lange, U. Huttner, D. Golde, T. Meier, M. Kira, S. W. Koch *et al.*, Sub-cycle control of terahertz high-harmonic generation by dynamical Bloch oscillations, Nat. Photonics **8**, 119 (2014).

[4] M. Hohenleutner, F. Langer, O. Schubert, M. Knorr, U. Huttner, S. W. Koch, M. Kira, and R. Huber, Real-time observation of interfering crystal electrons in high-harmonic generation, Nature (London) **523**, 572 (2015).

[5] G. Vampa, T. J. Hammond, N. Thiré, B. E. Schmidt, F. Légaré, C. R. McDonald, T. Brabec, D. D. Klug, and P. B. Corkum, All-optical reconstruction of crystal band structure, Phys. Rev. Lett. **115**, 193603 (2015).

[6] F. Langer, M. Hohenleutner, C. P. Schmid, C. Poellmann, P. Nagler, T. Korn, C. Schüller, M. S. Sherwin, U. Huttner, J. T. Steiner *et al.*, Lightwave-driven quasiparticle collisions on a subcycle timescale, Nature (London) **533**, 225 (2016).

[7] Y. S. You, D. A. Reis, and S. Ghimire, Anisotropic high-harmonic generation in bulk crystals, Nat. Phys. **13**, 345 (2017).

[8] N. Yoshikawa, T. Tamaya, and K. Tanaka, High-harmonic generation in graphene enhanced by elliptically polarized light excitation, Science **356**, 736 (2017).

[9] H. Lakhotia, H. Y. Kim, M. Zhan, S. Hu, S. Meng, and E. Goulielmakis, Laser picoscopy of valence electrons in solids, Nature (London) **583**, 55 (2020).

[10] F. Krausz and M. Ivanov, Attosecond physics, Rev. Mod. Phys. **81**, 163 (2009).

[11] G. Vampa, C. R. McDonald, G. Orlando, D. D. Klug, P. B. Corkum, and T. Brabec, Theoretical analysis of high-harmonic generation in solids, Phys. Rev. Lett. **113**, 073901 (2014).

[12] G. Vampa, C. R. McDonald, G. Orlando, P. B. Corkum, and T. Brabec, Semiclassical analysis of high harmonic generation in bulk crystals, Phys. Rev. B **91**, 064302 (2015).

[13] T. T. Luu and H. J. Wörner, High-order harmonic generation in solids: A unifying approach, Phys. Rev. B **94**, 115164 (2016).

[14] R. E. F. Silva, I. V. Blinov, A. N. Rubtsov, O. Smirnova, and M. Ivanov, High-harmonic spectroscopy of ultrafast many-body dynamics in strongly correlated systems, Nat. Photonics **12**, 266 (2018).

[15] N. Tancogne-Dejean, M. A. Sentef, and A. Rubio, Ultrafast modification of Hubbard *U* in a strongly correlated material: *Ab initio* high-harmonic generation in NiO, Phys. Rev. Lett. **121**, 097402 (2018).

[16] Y. Murakami, M. Eckstein, and P. Werner, High-harmonic generation in Mott insulators, Phys. Rev. Lett. **121**, 057405 (2018).

[17] Y. Murakami and P. Werner, Nonequilibrium steady states of electric field driven Mott insulators, Phys. Rev. B **98**, 075102 (2018).

[18] M. Lysne, Y. Murakami, and P. Werner, Signatures of bosonic excitations in high-harmonic spectra of Mott insulators, Phys. Rev. B **101**, 195139 (2020).

[19] S. Imai, A. Ono, and S. Ishihara, High harmonic generation in a correlated electron system, Phys. Rev. Lett. **124**, 157404 (2020).

[20] Y. Murakami, S. Takayoshi, A. Koga, and P. Werner, High-harmonic generation in one-dimensional Mott insulators, Phys. Rev. B **103**, 035110 (2021).

[21] Y. Murakami, K. Uchida, A. Koga, K. Tanaka, and P. Werner, Anomalous temperature dependence of high-harmonic generation in Mott insulators, Phys. Rev. Lett. **129**, 157401 (2022).

[22] M. R. Bionta, E. Haddad, A. Leblanc, V. Gruson, P. Lassonde, H. Ibrahim, J. Chaillou, N. Émond, M. R. Otto, A. Jiménez-Galán *et al.*, Tracking ultrafast solid-state dynamics using high harmonic spectroscopy, Phys. Rev. Res. **3**, 023250 (2021).

[23] O. Grånäs, I. Vaskivskyi, X. Wang, P. Thunström, S. Ghimire, R. Knut, J. Söderström, L. Kjellsson, D. Turenne, R. Y. Engel *et al.*, Ultrafast modification of the electronic structure of a correlated insulator, Phys. Rev. Res. **4**, L032030 (2020).

[24] K. Uchida, G. Mattoni, S. Yonezawa, F. Nakamura, Y. Maeno, and K. Tanaka, High-order harmonic generation and its unconventional scaling law in the Mott-insulating Ca_2RuO_4, Phys. Rev. Lett. **128**, 127401 (2022).

[25] Z. Jirák, S. Krupička, Z. Šimša, M. Dlouhá, and S. Vratislav, Neutron diffraction study of $Pr_{1-x}Ca_xMnO_3$ perovskites, J. Magn. Magn. Mater. **53**, 153 (1985).

[26] *Colossal Magnetoresistive Oxides*, edited by Y. Tokura (Gordon and Breach, London, 2000).

[27] M. Tokunaga, N. Miura, Y. Tomioka, and Y. Tokura, High-magnetic-field study of the phase transitions of $R_{1-x}Ca_xMnO_3$ (R = Pr, Nd), Phys. Rev. B **57**, 5259 (1998).

[28] C. N. R. Rao, A. R. Raju, V. Ponnambalam, S. Parashar, and N. Kumar, Electric-field-induced melting of the randomly pinned charge-ordered states of rare-earth manganates and associated effects, Phys. Rev. B **61**, 594 (2000).

[29] C. Cui and T. A. Tyson, Pressure effects on charge, spin, and metal-insulator transitions in the narrow bandwidth manganite $Pr_{1-x}Ca_xMnO_3$, Phys. Rev. B **70**, 094409 (2004).

[30] Y. Tomioka, A. Asamitsu, H. Kuwahara, Y. Moritomo, and Y. Tokura, Magnetic-field-induced metal-insulator phenomena in $Pr_{1-x}Ca_xMnO_3$ with controlled charge-ordering instability, Phys. Rev. B **53**, R1689(R) (1996).

[31] E. Dagotto, Complexity in strongly correlated electronic systems, Science **309**, 257 (2005).

[32] Y. Tokura, Critical features of colossal magnetoresistive manganites, Rep. Prog. Phys. **69**, 797 (2006).

[33] Y. Okimoto, Y. Tomioka, Y. Onose, Y. Otsuka, and Y. Tokura, Charge ordering and disordering transitions in $Pr_{1-x}Ca_xMnO_3$ ($x = 0.4$) as investigated by optical spectroscopy, Phys. Rev. B **57**, R9377(R) (1998).

[34] S. Mildner, J. Hoffmann, P. E. Blöchl, S. Techert, and C. Jooss, Temperature- and doping-dependent optical absorption in the small-polaron system $Pr_{1-x}Ca_xMnO_3$, Phys. Rev. B **92**, 035145 (2015).

[35] See Supplemental Material at http://link.aps.org/supplemental/10.1103/PhysRevResearch.6.L042032 for the schematic figures and supplemental results, which includes Refs. [2,3,36–41].

[36] H. Yada, Y. Ijiri, H. Uemura, Y. Tomioka, and H. Okamoto, Enhancement of photoinduced charge-order melting via anisotropy control by double-pulse excitation in perovskite manganites: $Pr_{0.6}Ca_{0.4}MnO_3$, Phys. Rev. Lett. **116**, 076402 (2016).

[37] A. Daoud-Aladine, J. Rodríguez-Carvajal, L. Pinsard-Gaudart, M. T. Fernández-Díaz, and A. Revcolevschi, Zener polaron ordering in half-doped manganites, Phys. Rev. Lett. **89**, 097205 (2002).

[38] O. Neufeld, D. Podolsky, and O. Cohen, Floquet group theory and its application to selection rules in harmonic generation, Nat. Commun. **10**, 405 (2019).

[39] L. Wu, R. F. Klie, Y. Zhu, and C. Jooss, Experimental confirmation of Zener-polaron-type charge and orbital ordering in $Pr_{1-x}Ca_xMnO_3$, Phys. Rev. B **76**, 174210 (2007).

[40] S. Ghimire, A. D. DiChiara, E. Sistrunk, G. Ndabashimiye, U. B. Szafruga, A. Mohammad, P. Agostini, L. F. DiMauro, and D. A. Reis, Generation and propagation of high-order harmonics in crystals, Phys. Rev. A **85**, 043836 (2012).

[41] L. Yue and M. B. Gaarde, Introduction to theory of high-harmonic generation in solids: Tutorial, J. Opt. Soc. Am. B **39**, 535 (2022).

[42] K. Chinzei and T. N. Ikeda, Disorder effects on the origin of high-order harmonic generation in solids, Phys. Rev. Res. **2**, 013033 (2020).